

BLIND SOURCE SEPARATION APPROACHES TO REMOVE IMAGING ARTEFACTS IN EEG SIGNALS RECORDED SIMULTANEOUSLY WITH FMRI

Bertrand Rivet^{1,2}, Guillaume Flandin³, Antoine Souloumiac², Jean-Baptiste Poline³

¹ GIPSA-Lab, CNRS-UMR 5216,
Grenoble Institute of Technology
46 avenue Félix Viallet,
38000 Grenoble, France

² CEA, LIST, Laboratoire Processus
Stochastiques et Spectres
CEA, Saclay,
Gif sur Yvette, F-91191, France

³ CEA, Neurospin, I2BM,
CEA, Saclay,
Gif sur Yvette, F-91191, France

ABSTRACT

Using jointly functional magnetic resonance imaging (fMRI) and electroencephalography (EEG) is a growing field in human brain mapping. However, EEG signals are contaminated during acquisition by imaging artefacts which are stronger by several orders of magnitude than the brain activity. In this paper¹, we propose three methods to remove the imaging artefacts based on the temporal and/or the spatial structures of these specific artefacts. Moreover, we propose a new objective criterion to measure the performance of the proposed algorithm on real data. Finally, we show the efficiency of the proposed methods applied to a real dataset.

1. INTRODUCTION

The combination of electroencephalography (EEG) and functional magnetic resonance imaging (fMRI) has recently been investigated in human brain imaging [1, 2, 3]. The fMRI modality provides signals related to the hemodynamic neuronal activity with a very high spatial resolution (around $2 \times 2 \times 2$ mm³) and with a low temporal resolution (around 3s). A contrario, the EEG modality provides signals related to the electrophysiological activity with a very high temporal resolution (around 1kHz) and with a low spatial resolution (from 32 to 512 scalp sensors). As a consequence, some studies investigated the possibility of using the strengths of these two techniques by combining their complementarities [2].

However, the EEG signals recorded during MRI acquisition contain two main types of artifacts due to the magnetic field used by the MRI scanner: the ballistocardiogram (BCG) and imaging artifacts. BCG artifact is related to cardiac rhythm and is mainly due to the heart-related blood and electrodes movements in the magnetic field. Imaging artifact is induced by the gradient magnetic fields used for spatial encoding in MRI. Different methods were proposed to attenuate these artifacts, see [1, 4, 3] for instance. They exploit separately the temporal structure of imaging artifact and/or the spatial structure of imaging. In this paper, we address the same problem of removing imaging artifact. The proposed methods also exploit the temporal and spatial structures of the imaging artifact but in different ways.

This paper is organized as follows. Section 2 describes the temporal and spatial structures of imaging artifact as well as the proposed methods to remove them. Section 3 presents the results that have been achieved whereas Section 4 concludes the paper with comments and perspectives.

2. IMAGING ARTEFACT REMOVAL

In this section, the temporal and spatial structures of imaging artefact are stressed and we explain how we propose to exploit them to remove imaging artefact in EEG signals.

The two main properties rest upon the fact that the imaging artifact reflects the switching of gradient magnetic field used to record MRI where a volume is composed of several slices, each of them representing an fMRI image. Firstly, since during a classical fMRI recording each volume is composed of identical slides, the associated gradient magnetic field is the same for each volume. Secondly, since all the EEG sensors are immersed in the same magnetic field, they record the same physical phenomenon in different ways.

As a consequence, on the first hand the effect of recording different volumes must have the same influence in the recorded EEG during the experiment, and on the other hand the imaging artefact must occupy a small spatial subspace of space spanned by the recorded EEG.

2.1 Temporal model of imaging artefact

Let $x_i(t)$ denote the EEG signal recorded by the i -th sensor at continuous time t . As explained above, the influence of artefact gradient may be modelled by

$$x_i(t) = \sum_j g_i(t - \tau_j) + e_i(t), \quad (1)$$

where τ_j is the j -th volume timing event, $g_i(t)$ is a function which expresses the imaging artefacts of one volume on the i -th sensor, and $e_i(t)$ is the term of ongoing brain activity. A classical approach to estimate $e_i(t)$ is first to estimate $g_i(t)$ and then to remove it from $x_i(t)$:

$$\hat{e}_i(t) = x_i(t) - \sum_j \hat{g}_i(t) * \delta(t - \tau_j), \quad (2)$$

where $*$ is the convolution product and $\delta(t)$ is the delta Dirac function. Under the assumption that EEG activity is uncorrelated if the time delay is larger than $\min(\tau_{n+1} - \tau_n)$, one can estimate $g_i(t)$ for each sensor by

$$\hat{g}_i(t) = \frac{1}{N} \sum_{k=0}^{N-1} x_i(t + \tau_k). \quad (3)$$

However, since we are dealing with discrete time signals, (3) becomes

$$\hat{g}_i[n] \triangleq \hat{g}_i(nT_s) = \frac{1}{N} \sum_{k=0}^{N-1} x_i \left(\left(n + \frac{\tau_k}{T_s} \right) T_s \right) \quad (4)$$

where T_s is the sampling period. The main difficulty comes from the asynchronously clocks of EEG and fMRI data: as

¹This work has been partially supported by CEA/DRT (Grant ACAV Open-Vibe).

a consequence τ_k/T_s is not necessary an integer, thus substituting τ_k/T_s by n_k , the closest integers to τ_k/T_s , leads to an awkward estimation of the imaging artefact. A common solution [1, 4, 3] is to interpolate the EEG data by oversampling to obtain a better estimation of τ_k . However, this solution suffers from two main drawbacks: over-sampled data require more memory and a high resampling rate is needed to obtain a good alignment. To overcome this, we propose to estimate τ_k and to time shift $x_i(t)$ without any oversampling thanks to the following property

$$\text{TF}(x(t - \tau)) = X(f) \exp(-i2\pi f\tau), \quad (5)$$

where $\text{TF}(\cdot)$ is the Fourier transform operator, $t^2 = -1$ and $X(f)$ is the Fourier transform of $x(t)$.

Let $\mathbf{x}_i^{(k)} = [x_i[n_k], \dots, x_i[n_k + N - 1]]^T$ be EEG signal during the acquisition of k -th volume and $\mathbf{X}_i^{(k)} = [X_i[0], \dots, X_i[N - 1]]^T$ its Fourier transform. Thus the cross-spectrum of $X_i^{(0)}[\mathbf{v}]$ and $X_i^{(k)}[\mathbf{v}]$ for all k is defined by

$$X_i^{(0)}[\mathbf{v}] \left(X_i^{(k)}[\mathbf{v}] \right)^* = \left(G_i^{(0)}[\mathbf{v}] + E_i^{(0)}[\mathbf{v}] \right) \times \left(G_i^{(k)}[\mathbf{v}] + E_i^{(k)}[\mathbf{v}] \right)^*,$$

where \cdot^* is the complex conjugate. Since the imaging artefact is much stronger than the ongoing brain activity and thanks to (5), and choosing arbitrary $\tau_0 = 0$, the cross-spectrum can be expressed as

$$X_i^{(0)}[\mathbf{v}] \left(X_i^{(k)}[\mathbf{v}] \right)^* \simeq \left| G_i^{(0)}[\mathbf{v}] \right|^2 \exp\left(i2\pi \frac{\mathbf{v}}{N} \tau_k'\right), \quad (6)$$

where $\tau_k' = \frac{\tau_k}{T_s} - n_k$. One can see that the phase of the cross-spectrum depends linearly on τ_k . Note that n_k is known thanks to the triggers received from the MRI machine which indicates the start of each volume. τ_k' is thus estimated by a linear regression on the phase for frequency bins in the pass-band of $g_i(t)$ defined by frequencies whose modulus amplitude $|G_i^{(0)}[\mathbf{v}]|^2$ represents a definite part of the power of $g_i(t)$ approximated by the power of $x_i(t)$ (typically more than 10%).

Finally, the imaging artefact is estimated by

$$\hat{g}_i[n] = \frac{1}{K} \sum_{k=0}^{K-1} \tilde{x}_i^{(k)}[n], \quad (7)$$

where $\tilde{x}_i^{(k)}[n]$ is the re-aligned observations obtained by the inverse Fourier transform of $X_i^{(k)}[\mathbf{v}] \exp(i2\pi \mathbf{v} \hat{\tau}_k'/N)$, and the ongoing brain activity $e_i[n]$ is estimated by

$$\hat{e}_i[n] = x_i[n] - \sum_j \hat{g}_i^{(j)}[n], \quad (8)$$

where $\hat{g}_i^{(j)}[n]$ is the inverse Fourier transform of $\hat{G}_i[\mathbf{v}] \exp(-i2\pi \mathbf{v} \hat{\tau}_j'/N)$. This algorithm to cancel the influence of imaging artefact on EEG signal is called Frequency Averaged Artefact Subtraction (F-AAS) and is resumed in Algorithm 1.

2.2 Spatial model of imaging artefact

The fact that all the sensors record the same physical phenomenon in different ways can be modeled by

Algorithm 1 F-AAS algorithm.

- 1: **for** each sensor i **do**
 - 2: Compute Fourier transform of $x_i^{(k)}[n] \Rightarrow X_i^{(k)}[\mathbf{v}]$
 - 3: **for** each volume k **do**
 - 4: Compute cross-spectrum (6): $X_i^{(0)}[\mathbf{v}] \left(X_i^{(k)}[\mathbf{v}] \right)^*$
 - 5: Estimate time delay τ_k' by linear regression on cross-spectrum phase
 - 6: Temporal alignment of $\mathbf{x}^{(k)}[n] \Rightarrow \tilde{\mathbf{x}}^{(k)}[n]$
 - 7: **end for**
 - 8: Estimate imaging artefact $\hat{g}_i[n]$ by (7)
 - 9: Estimate brain activity $\hat{e}_i[n]$ by (8)
 - 10: **end for**
-

$$\mathbf{x}[n] = A \mathbf{g}[n] + \mathbf{e}[n], \quad (9)$$

where $\mathbf{x}[n] = [x_1[n], \dots, x_{N_x}[n]]^T$ is the column vector of the recorded signals, $\mathbf{g}[n] = [g_1[n], \dots, g_{N_g}[n]]^T$ is the column vector expressing the imaging artefact and $\mathbf{e}[n] = [e_1[n], \dots, e_{N_x}[n]]^T$ is the column vector of the ongoing brain activity. $A \in \mathbb{R}^{N_x \times N_g}$ is the mixing matrix. Model (9) is thus a linearly instantaneous mixture which can be inverted by independent component analysis (ICA) [5]. It aims at finding a separation matrix B such that $\mathbf{y}[n] = B \mathbf{x}[n]$ is a vector with mutually independent components. Most of used ICA algorithms for EEG signal processing are based on non-Gaussianity [6, 7] or based on time coherence [8]. To estimate separation matrix B , we propose to exploit the non-stationarity of the imaging artefact: as can be seen on Fig. 3(a), the imaging artefact on EEG signals is only present during the recording of volumes. If the sources are assumed to be mutually independent (or at least uncorrelated), covariance matrices $C_{yy}(n)$ of signal $\mathbf{y}[n]$ at several time indexes n must be diagonal. A basic criterion for blind source separation (BSS) [9] is to compute $C_{xx}(n)$ from the observations $\mathbf{x}[n]$ and then to adjust matrix B such that $C_{yy}(n)$ is as diagonal as possible. Since this condition must be verified for any time index n , this can be done by a joint-diagonalisation method, and in the following we use the algorithm of [10]. Among the estimated sources $y_i[n]$, we proposed to select those which contain imaging artefact: let $\mathcal{T}_g \subset \{1, \dots, N_s\}$ denote this set of N_g indexes. Then, the F-AAS algorithm is applied on each source $y_i[n]$ if $i \in \mathcal{T}_g$, and each source $y_i[n]$ such that $i \notin \mathcal{T}_g$ are kept unaltered. Finally, the brain activity is estimated by

$$\hat{\mathbf{e}}[n] = B^{-1} \mathbf{y}'[n], \quad (10)$$

where $\mathbf{y}'[n]$ is the vector composed of the unselected estimated sources ($y_i(t)$, with $i \notin \mathcal{T}_g$) plus the estimated sources ($y_i(t)$, with $i \in \mathcal{T}_g$) denoised by F-AAS algorithm.

We call this procedure Spatial Averaged Artefact Subtraction (S-AAS), and it is summarized in Algorithm 2. Note that this second approach seems more conservative than F-AAS applied directly on all sensors $\mathbf{x}[n]$. Indeed, F-AAS algorithm may result in the modification of brain activity EEG data. However to express EEG data as $\mathbf{x}[n]$ in the sensor space (9) or to express them as $\mathbf{y}[n]$ in the source space is equivalent since estimated matrix B is invertible. Moreover the imaging artefact results from the magnetic field thus its dimension must be reduced compared to the numbers of EEG sensors. As a result, ICA may concentrate the influence of this magnetic field in a limited number of components

$N_g < N_s$. S-AAS algorithm finally keeps unaltered $N_s - N_g$ signals, minimizing the eventual awkward influences of F-AAS.

Algorithm 2 S-AAS algorithm.

- 1: Compute a set of covariance matrices $\{C_{xx}(n)\}_n$
 - 2: Estimate matrix B by joint-diagonalization of $\{C_{xx}(n)\}_n$
 - 3: Compute estimated sources: $\mathbf{y}[n] = B\mathbf{x}[n]$
 - 4: Select sources contaminated by imaging artefact $\Rightarrow \mathcal{T}_g$
 - 5: **for** each source i **do**
 - 6: **if** $i \in \mathcal{T}_g$ **then**
 - 7: Apply F-AAS algorithm on $y_i[n] \Rightarrow y'_i[n]$ obtained by (8)
 - 8: **else**
 - 9: Keep unaltered $y_i[n] \Rightarrow y'_i[n] = y_i[n]$
 - 10: **end if**
 - 11: **end for**
 - 12: Estimate brain activity $\hat{\mathbf{e}}[n]$ by (10)
-

2.3 Spatio-temporal model of imaging artefact

As explained in Subsections 2.1 and 2.2, the imaging artefact has a temporal structure and a spatial structure. This spatio-temporal structure can then be modelled as a convolutive mixture

$$\mathbf{x}(t) = A(t) * \mathbf{g}(t) + \mathbf{e}(t), \quad (11)$$

where $A(t)$ is the mixing filter matrix whose (k, l) -th entry is expressed as $\sum_j A_{k,l}^{(j)} \delta(t - \tau_j)$: $A(t) = \sum_j A^{(j)} \times \delta(t - \tau_j)$. One can then estimate $\mathbf{g}(t)$ thanks to a separating filter matrix $B(t)$ by

$$\hat{\mathbf{g}}(t) = B(t) * \mathbf{x}(t), \quad (12)$$

where $B(t)$ can be expressed as

$$B(t) = \sum_j B^{(j)} \delta(t + \tau_j). \quad (13)$$

First, to overcome the problem of asynchronous clocks between EEG and MRI data, the same estimation of τ_j than proposed in Subsection 2.1 is used. Second, to enforce the impulse response of $B(t)$ to have the special structure (13), the observations $\mathbf{x}^{(k)}[n]$ are first computed and time shifted to obtain $\tilde{\mathbf{x}}^{(k)}[n]$. Then block Toeplitz matrix $Z \in \mathbb{R}^{(N_x J) \times (N_x K)}$ is computed such that

$$Z = \begin{pmatrix} \tilde{\mathbf{x}}_1^{(0)T} & \tilde{\mathbf{x}}_1^{(1)T} & \dots & \tilde{\mathbf{x}}_1^{(K-1)T} \\ \vdots & \vdots & \ddots & \vdots \\ \tilde{\mathbf{x}}_{N_x}^{(0)T} & \tilde{\mathbf{x}}_{N_x}^{(1)T} & \dots & \tilde{\mathbf{x}}_{N_x}^{(K-1)T} \\ \vdots & \vdots & \ddots & \vdots \\ \tilde{\mathbf{x}}_1^{(J-1)T} & \tilde{\mathbf{x}}_1^{(J)T} & \dots & \tilde{\mathbf{x}}_1^{(J+K-2)T} \\ \vdots & \vdots & \ddots & \vdots \\ \tilde{\mathbf{x}}_{N_x}^{(J-1)T} & \tilde{\mathbf{x}}_{N_x}^{(J)T} & \dots & \tilde{\mathbf{x}}_{N_x}^{(J+K-2)T} \end{pmatrix}, \quad (14)$$

where $\tilde{\mathbf{x}}_i^{(k)} = [\tilde{x}_i^{(k)}[0], \dots, \tilde{x}_i^{(k)}[N-1]]^T$. Finally, separating filters matrix $B(t)$ is estimated thanks to the non-stationary blind source separation method presented in Subsection 2.2 applied on $Z' \in \mathbb{R}^{J' \times (N_x K)}$, which is obtained from Z by a principal component analysis (PCA) to reduce the dimension of matrix Z : $Z' = WZ$, where $W \in \mathbb{R}^{J' \times (N_x J)}$ is the

product of the whitening matrix by the projection matrix on the main principal components. Joint-diagonalisation process provides a matrix R such that the components of $\mathbf{y}[n]$ defined by

$$\mathbf{y}[n] = R\mathbf{z}'[n], \quad (15)$$

where $\mathbf{z}'[n]$ is the n -th column of Z' , are more independent.

$B(t)$ is then deduced from R by $B_{kl}^{(j)} = (RW)_{k,(j-1)N_x+l}$. Among the estimated sources $y_i[n]$, let \mathcal{T}_g be the set of indexes corresponding to the imaging artefact sources. The brain activity is then estimated from raw data $\mathbf{x}[n]$ by

$$\hat{\mathbf{e}}[n] = \mathbf{x}[n] - ((RW)_{\mathcal{T}_g,:}^T (RW)_{\mathcal{T}_g,:})^{-1} (RW)_{\mathcal{T}_g,:}^T \mathbf{z}[n], \quad (16)$$

where $(RW)_{\mathcal{T}_g,:}$ denotes the sub-matrix of (RW) with all the columns and the rows indexes in \mathcal{T}_g . This algorithm is denoted Spatio-Temporal Average Artefact Subtraction (ST-AAS) and it is resumed in Algorithm 3.

Algorithm 3 ST-AAS algorithm.

- 1: **for** each volume k **do**
 - 2: Temporal alignment of $\mathbf{x}^{(k)}[n] \Rightarrow \tilde{\mathbf{x}}^{(k)}[n]$
 - 3: **end for**
 - 4: Compute matrix Z (14)
 - 5: PCA of $Z \Rightarrow W$ and $\mathbf{z}'[n]$
 - 6: Compute a set of covariance matrices $\{C_{z'z'}(n)\}_n$
 - 7: Estimate R by joint-diagonalisation
 - 8: Select sources contaminated by imaging artefact $\Rightarrow \mathcal{T}_g$
 - 9: Estimate brain activity $\hat{\mathbf{e}}[n]$ by (16)
-

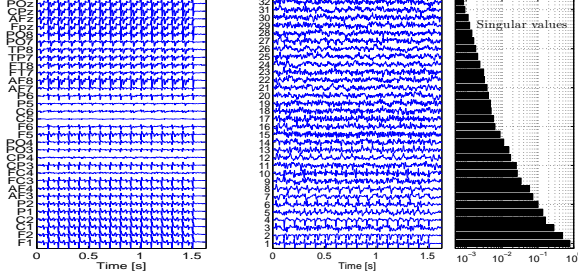
3. RESULTS

In this section, the data acquisition process and the results obtained by the proposed methods are presented.

3.1 Data acquisition

EEG was acquired using the MRI-compatible BrainAmp MR (BrainProducts, Munich, Germany) EEG amplifier and the BrainCap electrode cap (EasyCap, Herrsching-Breitbrunn, Germany) with sintered Ag/AgCl non-magnetic ring electrodes providing 32 EEG channels. They were positioned according to the classic 10-20 system. Raw EEG was sampled at 5kHz using the BrainVision Recorder software (BrainProducts) with a signal range +/-16mV (16-bit sampling). A 7-minute session was recorded inside the MRI environment during image acquisition while the subject was presented a visual stimulation (flashing rings with a perceived frequency of 5Hz). EEG data were hardware filtered using a low-pass filter (fc=250 Hz), an high-pass filter (fc=0.016Hz) and a notch-filter around 50Hz. Functional MRI images were acquired on a 3T Trio scanner (Siemens, Erlangen, Germany) with a standard head coil using an Echo Planar Imaging (EPI) sequence covering almost the entire brain (TR=45mss + 1.5s gap, TE=45, 64 axial slices, voxel size $3.75 \times 3.75 \times 5$ mm³, 2 mm gap). This sparse acquisition allows us to have a 1.5 second window gradient artefact free followed by a 1.5 second of artefacted signal for each fMRI volume. Importantly, there was no synchronisation between the MR sequence and the EEG amplifier clocks.

Before applying the proposed methods, the raw EEG signals were first 1Hz high-pass filtered by a 2nd order forward-backward Butterworth filter. After the estimation of time delay between volumes, the high-pass filtered signals were



(a) Averaged imaging artefact

(b) Singular components

Figure 1: F-AAS algorithm. Fig. 1(a) estimation of the averaged imaging artefact $\hat{g}_i[n]$ (7). Fig. 1(b) singular components of the averaged imaging artefact (each component is normalized to have a unit standard deviation).

60Hz low-pass filter by a 2nd order forward-backward Butterworth filter. One can see (Fig. 3(a)) that this low-pass filtering attenuates the imaging artefacts without cancelling them.

3.2 Problem of quality estimation criterion

Using data recorded in real condition leads to the problem of the quality of the estimation. Indeed, since the artefact-free signals are unknown there is no general objective index to evaluate the estimations. To overcome this difficulty, we propose to use a new index based on the generalized eigenvalues. Indeed, let \mathcal{N}_1 and \mathcal{N}_2 be two set of time indexes. Let $C_x(\mathcal{N}_1)$ and $C_x(\mathcal{N}_2)$ be two covariance matrices of $\mathbf{x}[n]$ with $n \in \mathcal{N}_1$ and $n \in \mathcal{N}_2$, respectively. If $\mathbf{x}[n]$ is stationary then the generalized eigenvalues of couple $(C_x(\mathcal{N}_1), C_x(\mathcal{N}_2))$ are equal to one. If some components of $\mathbf{x}[n]$ are more powerful during \mathcal{N}_1 , then some of the generalized eigenvalue are greater than one [11]. We thus propose a new criterion to evaluate the estimations. Let \mathcal{N}_g be the set of time indexes corresponding of the MRI acquisition. Let \mathcal{N}_f be the set of time indexes corresponding artefact-free samples (*i.e.* between MRI acquisitions). And let finally \mathcal{N}_{f_1} and \mathcal{N}_{f_2} be two disjoint subsets of $\mathcal{N}_f = \mathcal{N}_{f_1} \cup \mathcal{N}_{f_2}$, with the same cardinal. The proposed performance index is thus defined by comparing the two following set of generalized eigenvalues (GEV)

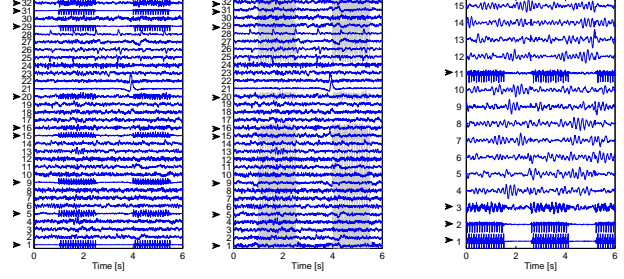
$$PI_1 = \{ \text{GEV of } (C_x(\mathcal{N}_{f_1}), C_x(\mathcal{N}_{f_2})) \} \quad (17)$$

$$PI_2 = \{ \text{GEV of } (C_{\hat{e}}(\mathcal{N}_g), C_x(\mathcal{N}_f)) \}. \quad (18)$$

Indeed, if the two sets PI_1 and PI_2 are equivalent this means that the imaging artefact removal is efficient. A contrario, if the 2nd order statistics of $\hat{\mathbf{e}}[n]$ are different between \mathcal{N}_g and \mathcal{N}_f , then these two subset are quite different, as one can see for the low-pass filtered observations $\mathbf{x}[n]$ (Fig. 3(e)).

3.3 Gradient artefact removal

The F-AAS algorithm (Subsection 2.1) was first applied on the EEG data (Fig. 1). The averaged imaging artefact $\hat{g}_i[n]$ (7) (with $K = 20$) for each sensor is plotted in Fig. 1(a). One can see that the influence of the imaging gradient is different for each sensor but seems spatially redundant. This is confirmed by a principal component analysis: the first four



(a) Sources estimated by S-AAS before (left) and after (right) additional F-AAS

(b) Sources estimated by ST-AAS

Figure 2: Estimated sources by S-AAS and ST-AAS, Fig. 2(a) and 2(b), respectively. Note that each source is normalized separately to have a unit standard deviation so they do not have the same ordinate axis. The gray plots are the estimated sources before the additional F-AAS algorithm.

principal components represent 96% of the total variance. The result of the F-AAS algorithm is shown in Fig. 3(b). The proposed method is efficient to remove imaging artefact (Fig. 3(f)): the two performances indexes PI_1 and PI_2 are quite equivalent.

In a second experiment, the S-AAS algorithm (Subsection 2.2) was applied on the data. One can see on Fig. 2(a) that the blind source separation concentrates the imaging artefact in a limited number of components (nine indicated by arrows). This fact confirms once again that the imaging artefact have a spatial structure which can be enhanced by a spatial filtering. The F-AAS algorithm applied on these specific components efficiently remove the imaging artefact (Fig. 2(a)) which is confirmed by the final result shown in Fig. 3(c) and 3(g). In this experiment and in the following, the sources which contain imaging artefacts are selected manually. Actually this selection could be done automatically with a short term power criterion for instance.

In the last experiment, the ST-AAS algorithm (Subsection 2.3) was applied on the data. Matrix Z was computed with $J = 38$ and $K = 5$ leading to a 1216×65000 matrix Z since $N = 13000$. During the PCA stage, matrix Z is reduced to a 15×65000 matrix Z' , leading thus to 15 estimated sources $y_i[n]$ plotted in Fig. 2(b). One can see that most of the imaging artefact is concentrated in four sources (indicated by arrows) which were thus removed from the observations $\mathbf{x}[n]$. The final result of ST-AAS is shown in Fig. 3(d) and 3(h). Quite surprisingly, this algorithm seems to have less performance than F-AAS and S-AAS. This might be explained by the fact that this algorithm is a bite more difficult to use since it needs to fix more parameters (J , K and J' the number of principal components kept).

Finally, the three proposed algorithms seems to have quite good performance. On the first hand, F-AAS and S-AAS have a similar computational cost but, as already mentioned (Subsection 2.2), S-AAS seems more conservative and thus seems better (Fig. 3(f) and 3(g)). The two sets PI_1 and PI_2 are closer using S-AAS algorithm than using F-AAS. On the other hand, the ST-AAS has a higher computational cost and has little bit less good performance (Fig. 3(h)). Indeed, one can see that three largest GEV are quite different.

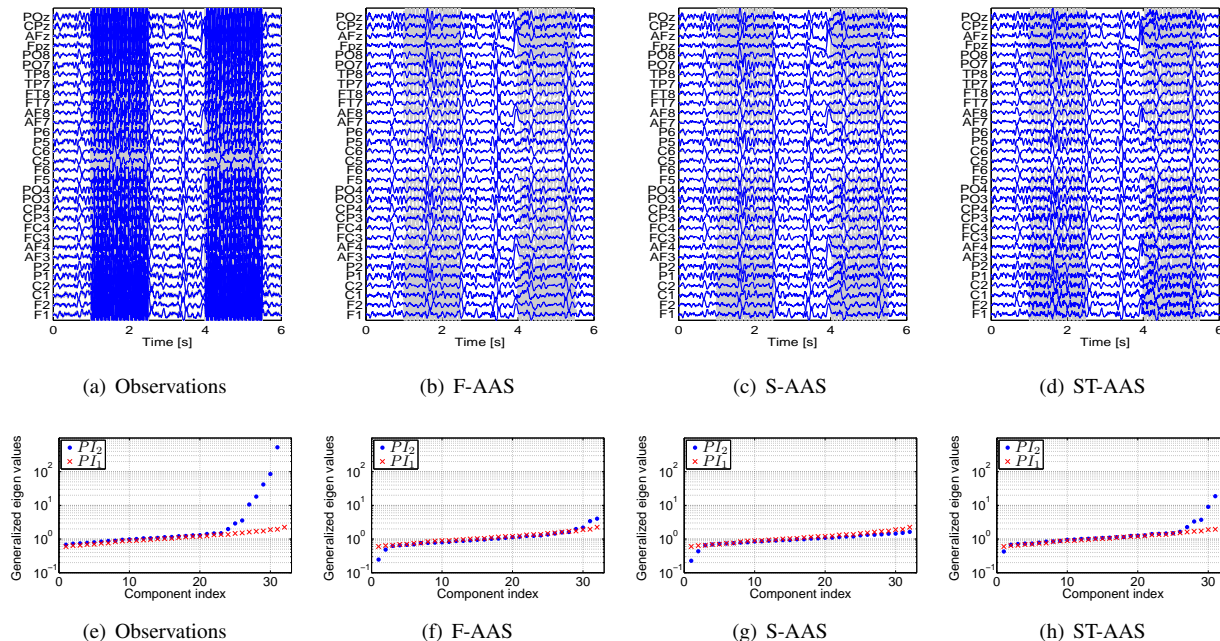


Figure 3: Estimated brain activity after removal of imaging artefact. Fig. 3(a): observations $\mathbf{x}[n]$ before (blue lines) and after (gray lines) the low-pass filtering. Fig. 3(b), Fig. 3(c) and Fig. 3(d) the blue lines represent the estimated brain activity $\hat{\mathbf{e}}[n]$ by F-AAS, S-AAS and ST-AAS algorithms, respectively. The gray lines show the low-pass filtered observations. Fig. 3(e), 3(f), 3(g), 3(h) show the two set of generalized eigenvalues PI_1 (red crosses) and PI_2 (blue points).

4. CONCLUSIONS AND PERSPECTIVES

In this preliminary study, we proposed three complementary algorithms based on spatial and/or temporal structures to remove imaging artefact. They have shown to be efficient on the recorded dataset. However, the more complete method (ST-AAS), which exploits the spatial and temporal structures of the imaging artefact, is slightly disappointing even if the S-AAS and the F-AAS algorithms, which exploit separately the temporal and spatial structures, seem to show that exploiting jointly spatial and temporal structures should be relevant. We are currently investigating new implementation to take into account the spatio-temporal structure of imaging artefact to improve the ST-AAS algorithm.

Moreover, even if the evaluation on real data is an open problem, the proposed objective criterion seems to be quite efficient to measure the performance of imaging artefact removal on real data. Finally, to be complete, the proposed methods have to be validated on other databases.

REFERENCES

- [1] P. J. Allen, O. Josephs, and R. Turner, "A Method for Removing Imaging Artifact from Continuous EEG Recorded during Functional MRI," *NeuroImage*, vol. 12, no. 2, pp. 230–239, Aug. 2000.
- [2] P.-J. Lahaye, S. Baillet, J.-B. Poline, and L. Garnero, "Fusion of simultaneous fMRI/EEG data based on the electro-metabolic coupling," in *Biomedical Imaging: Macro to Nano, 2004. IEEE International Symposium on*, 15–18 April 2004, pp. 864–867 Vol.1.
- [3] D. Mantini, M. Perrucci, S. Cugini, A. Ferretti, G. Romani, and C. Del Gratta, "Complete artifact removal for EEG recorded during continuous fMRI using independent component analysis," *NeuroImage*, vol. 34, no. 2, pp. 598–607, Jan. 2007.
- [4] R. Niazy, C. Beckmann, G. Iannetti, J. Brady, and S. Smith, "Removal of FMRI environment artifacts from EEG data using optimal basis sets," *NeuroImage*, vol. 28, no. 3, pp. 720–737, Nov. 2005.
- [5] P. Comon, "Independent component analysis, a new concept?" *Signal Processing*, vol. 36, no. 3, pp. 287–314, April 1994.
- [6] J.-F. Cardoso and A. Souloumiac, "Blind beamforming for non Gaussian signals," *IEE Proceedings-F*, vol. 140, no. 6, pp. 362–370, December 1993.
- [7] A. Hyvärinen and E. Oja, "A Fast Fixed-Point Algorithm for Independent Component Analysis," *Neural Computation*, vol. 9, no. 7, pp. 1483–1492, 1997.
- [8] A. Belouchrani, K. Abed-Meraim, and J.-F. Cardoso, "A blind source separation technique using second-order statistic," *IEEE Transactions on Signal Processing*, vol. 45, no. 2, pp. 434–444, February 1997.
- [9] D.-T. Pham, C. Servière, and H. Boumaraf, "Blind separation of speech mixtures based on nonstationarity," in *Proc. ISSPA'03*, Paris, France, July 2003.
- [10] D.-T. Pham, "Joint approximate diagonalization of positive definite matrices," *SIAM J. Matrix Anal. And Appl.*, vol. 22, no. 4, pp. 1136–1152, 2001.
- [11] A. Souloumiac, "Blind source detection and separation using second order non-stationarity," in *Proc. ICASSP*, vol. 3, Detroit, USA, May 1995, pp. 1912–1915.